Optical Fiber Technology 84 (2024) 103776

Contents lists available at ScienceDirect

Optical Fiber Technology

journal homepage: www.elsevier.com/locate/yofte

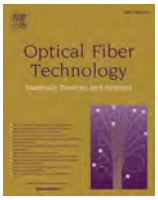

Single-polarization dual-hollow-core anti-resonant fiber coupler by polarized mode filtered method

Donglian Hou [a,1], Haoqiang Jia [a,1], Xing Wang [a], Xinzhi Sheng [b], Lu Xue [b], Paul K. Chu [c], Shuqin Lou [a,*]

[a] Key Laboratory of Communication and Information Systems, Beijing Municipal Commission of Education, School of Electronic and Information Engineering, Beijing Jiaotong University, Beijing, 100044, China
[b] School of Physical Science and Engineering, Beijing Jiaotong University, Beijing, 100044, China
[c] Department of Physics, Department of Materials Science & Engineering, and Department of Biomedical Engineering, City University of Hong Kong, Tat Chee Avenue, Kowloon, Hong Kong, China

ARTICLE INFO

Keywords:
Single-polarization coupler
Gyroscopes
Anti-resonant fibers
Dual-core fiber
Polarization extinction ratio

ABSTRACT

A single-polarization (SP) coupler based on a dual-hollow-core anti-resonant fiber (DHC-ARF) by polarized mode filtered method is proposed. The DHC-ARF is composed of ten cladding tubes with each core surrounded by five cladding tubes. By introducing cladding tubes with two different thicknesses along the two orthogonal directions, one polarized mode can be filtered out due to its high confinement loss caused by the mode coupling with the dielectric mode in the cladding wall, while another polarized mode with a low confinement loss can be maintained. By optimizing the structural parameters of the DHC-ARF, the confinement loss of the high-loss polarized mode is 50.44 dB/cm and that of the low-loss polarized mode is only 0.24 dB/cm at a wavelength of 1550 nm. By using a 1.52 cm long DHC-ARF, the SP coupler can be implemented with an operational bandwidth of 11 nm spanning the wavelength range between 1545 nm and 1556 nm, in which the polarization extinction ratio (PER) is less than −20 dB, the coupling ratio (CR) stabilizes to 50 ± 0.6 %, and the loss of the coupler is less than 0.44 dB. At the wavelength of 1550 nm, the lowest PER of −91.7 dB is achieved, while the CR and loss are 50 % and 0.37 dB, respectively. Furthermore, empirical formulas are derived for the structural parameters and wavelength, making it possible to predict the structural parameters of a DHC-ARF in the development of SP couplers for the expected wavelength. High-performance hollow-core SP coupler is significantly important to develop high-precision resonant HCF gyroscopes.

1. Introduction

The resonator fiber optic gyroscope (RFOG) has immense potential as a high-accuracy inertial rotation sensor for navigation [1]. Compared to the interferometric fiber-optic gyro, the RFOG has a smaller size, lower cost, and excellent linearity over a broad dynamic range [2,3]. Hollow-core fibers (HCFs) have been proposed for use in the fiber ring resonator (FRR) of the RFOGs to reduce the thermal polarization instability, backscattering, Kerr effect, Shupe effect, and Faraday effect in conventional solid-core fibers [4–8]. Despite the great promise of HCFs in RFOGs, the lack of HCF-based components has hampered wider applications and commercial development of HCFs [9,10].

The rotation rate of an RFOG is linearly proportional to the resonant frequency difference between the clockwise and counterclockwise modes of an eigenstate of polarization (ESOP) in the FRR and therefore, a primary ESOP is purposely excited in most RFOGs [11]. However, in practice, it is difficult to avoid occasional power coupling to the secondary ESOP due to environmental perturbations like uneven stresses, bending, and twisting [12]. To suppress the secondary ESOP caused by the unwanted coupling, polarization-maintaining fibers have been developed and implemented in RFOGs [13–15]. Owing to the absence of HCF-based couplers, solid-core fiber couplers are usually used to close the HCF-based FRR, thus giving rise to large Fresnel reflection (>3.5 %) at the silica-air interface between the solid-core fiber coupler and HCFs. An HCF-based single-polarization (SP) coupler that only permits the primary ESOP propagation is considered the ultimate solution in this

* Corresponding author.
E-mail address: shqlou@bjtu.edu.cn (S. Lou).
[1] These authors contributed equally to this work.

https://doi.org/10.1016/j.yofte.2024.103776
Received 2 February 2024; Received in revised form 1 March 2024; Accepted 29 March 2024

respect [16].

Dual-core fibers provide an attractive and powerful platform to guide and manipulate polarizations. Various fiber components can be made from dual-core fibers, for instance, polarization-maintaining couplers, polarization splitters, and polarization-insensitive couplers [17–23]. To develop an SP coupler based on the dual-core fiber, there is only one allowed polarized mode to couple between the two cores of dual-core fiber, whereas the other polarized mode is either forbidden from the coupling or suffers from a high loss. The coupling mechanism of dual-hollow-core fibers (DHCF) including dual-hollow-core photonic bandgap fibers (DHC-PBGFs) and dual-hollow-core anti-resonant fibers (DHC-ARFs) has been studied theoretically and experimentally. Ma *et al.* have demonstrated that the mode coupling of one polarized mode can be suppressed by exploiting the decoupling phenomenon in the DHC-PBGF, while the other polarized mode couples efficiently between the two cores [16]. Consequently, an SP coupler comprising the decoupled DHC-PBGF with a polarization extinction ratio (PER) greater than 30 dB at 1550 nm has been proposed. The DHC-PBGF-based SP coupler shows an obvious wavelength dependence as the high PER is only obtained at 1550 nm. Recently our group has demonstrated the decoupling phenomenon in DHC-ARFs [24] and designed an SP coupler based on the decoupled DHC-ARF with a high PER of −64.12 dB at 1550 nm, but the SP coupler shows a narrow bandwidth of only 4.4 nm [25]. The two aforementioned decoupled DHCF-based SP couplers show an operating bandwidth of only a few nanometers because the decoupling phenomenon in DHCFs depends on the core diameter, cladding wall, and periodic cladding structure of the fibers, consequently presenting some manufacturing challenges as well [26]. In contrast, the property of SP has been studied by filtering the polarized mode in single-core HCFs [27–30]. There are several designs of SP-HCFs and polarization filters based on HCFs. For instance, V. Serrão *et al.* have designed an SP hollow-core photonic bandgap fiber with a bandwidth of 11 nm by introducing a high air-filling fraction into the lattice of the fiber, so that the unwanted polarized mode experiences a high loss [27]. We have also introduced different cladding walls to filter one polarized mode of a single-core HC-ARF and proposed an SP HC-ARF with an operating bandwidth of up to 8 nm [29]. Recently, Zang *et al.* have fabricated an HCF-based polarization filter with a bandwidth of 14 nm by controlling the cladding tube thickness of the single-core HC-ARF [31]. However, although the simulation and experimental results have verified the feasibility of HC-ARF-based SP components by filtering one polarized mode in the fiber, it is still a challenge for the DHC-ARF-based component to filter effectively a polarized mode.

Herein, an SP coupler based on a DHC-ARF is designed and analyzed. By introducing two kinds of cladding tubes with different wall thicknesses along two orthogonal directions, one polarized mode can be filtered due to its high confinement loss (*CL*), while another polarized mode is maintained with a low *CL*. Numerical result shows that the *CL*s of two polarized mode are 50.44 dB/cm and 0.24 dB/cm at 1550 nm, respectively. By using a 1.52 cm long DHC-ARF, an SP coupler can be implemented with an operational bandwidth of 11 nm covering the wavelength range between 1545 nm and 1556 nm, in which the PER is less than −20 dB, the coupling ratio (CR) stabilizes within 50 ± 0.6 %, and the loss of the coupler is less than 0.44 dB. At a wavelength of 1550 nm, the lowest PER reaches −91.7 dB with the CR stabilizing at 50 % together with a loss of 0.37 dB. By analyzing the impact of the wall thicknesses and diameter of the cladding tubes on the *CL* of the fiber, empirical formulas are generated to predict the structural parameters of a DHC-ARF to aid the design and development of SP couplers. This high-performance hollow-core SP coupler is significantly important to develop high-precision resonant HCF gyroscopes.

2. Fiber structure and operation principle

Fig. 1(a) illustrates the cross-section of the DHC-ARF. The fiber comprises ten cladding tubes, in which the two cores are formed by eight

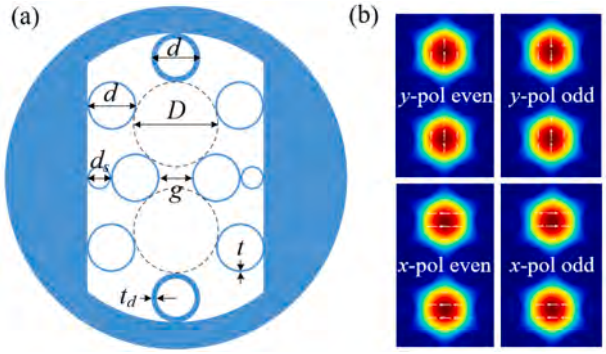

Fig. 1. Cross-section of the DHC-ARF (a) and modal fields of the four fundamental supermodes (b).

cladding tubes with a diameter of *d*, and the other two cladding tubes with a diameter of d_s are used to support the two cladding tubes between the two cores. Among the ten cladding tubes, two cladding tubes located in the *y*-direction have a thick wall with a thickness of t_d and the wall thickness of the other eight cladding tubes is denoted as *t*. The thick cladding wall t_d is aimed to filter the secondary ESOP. The two cores have the same diameter *D*. The DHC-ARF is made of pure silica and its refractive index is obtained by the Sellmeier formula. The initial parameters t_d, *t*, *d*, *D*, and d_s are set as 0.83 μm, 0.5 μm, 12.5 μm, 25 μm, and 6.8 μm, respectively.

The modal characteristics of the DHC-ARF are investigated by the finite-element method. A perfectly matched layer boundary is placed outside the fiber domain to accurately derive the fiber modal characteristics. The simulations are performed by using extremely fine mesh sizes of $\lambda/6$, $\lambda/4$, and $\lambda/4$ in the silica walls, air regions, and perfectly matched layer, where λ is the wavelength. Two pairs of fundamental supermodes exist in the DHC-ARFs, namely the *y*-polarized (*y*-pol) odd mode, *y*-pol even mode, *x*-polarized (*x*-pol) odd mode, and *x*-pol even mode. The electric field distributions of the four fundamental supermodes are presented in Fig. 1(b). In this way, the coupling length (L_c) is defined as a propagation length over which the light power in one core can be completely transferred to the other core. The confinement loss can also be obtained. For the *x*- and *y*-pol modes, $L_c^{x(y)}$ and $CL_{x(y)}$ are expressed by the following equations:

$$L_c^{x(y)} = \lambda/(2\left|\Delta \mathrm{Re}(n_{\mathrm{eff}}^{x(y)})\right|) \tag{1}$$

$$CL_{x(y)} = 20\lg e^{\alpha_{x(y)}} \tag{2}$$

where $\Delta \mathrm{Re}\left(n_{eff}^{x(y)}\right)$ denotes the difference of the real part of the effective refractive index (n_{eff}) between a pair of *x*(*y*)-pol supermodes, $\alpha_{x(y)}$ is the average attenuation constant of a pair of *x*(*y*)-pol supermodes, and α is calculated by $k_0\mathrm{Im}(n_{\mathrm{eff}})$, where k_0 and $\mathrm{Im}(n_{\mathrm{eff}})$ are the wave vector and imaginary part of n_{eff}, respectively.

The *x*- and *y*-pol modes are set as the primary ESOP and secondary ESOP, respectively. To obtain a DHC-ARF that can be used to develop the SP coupler, the key is to increase the confinement loss of the *y*-pol mode (CL_y) while maintaining a low confinement loss for the *x*-pol mode (CL_x). As the wall thickness of HC-ARFs greatly affects the air-guiding characteristics of the fiber, we first investigate the effect of the wall thickness t_d on CL_y and CL_x at 1550 nm. Fig. 2(a) shows that the CL_y and CL_x change with t_d. The loss peaks over 20 dB/cm appear from the CL_x and CL_y curves at t_d = 787.6 nm and t_d = 830 nm, respectively. At t_d = 787.6 nm, the CL_y is 11.36 dB/cm and the CL_x increases to 32.76 dB/cm. At t_d = 830 nm, the CL_y increases to 50.44 dB/cm, while the CL_x is only 0.25 dB/cm, indicating that the *x*-pol mode can be maintained and the *y*-pol mode is suppressed effectively. The loss peaks are caused by the impact of the dielectric modes on the core modes. As shown in the Re

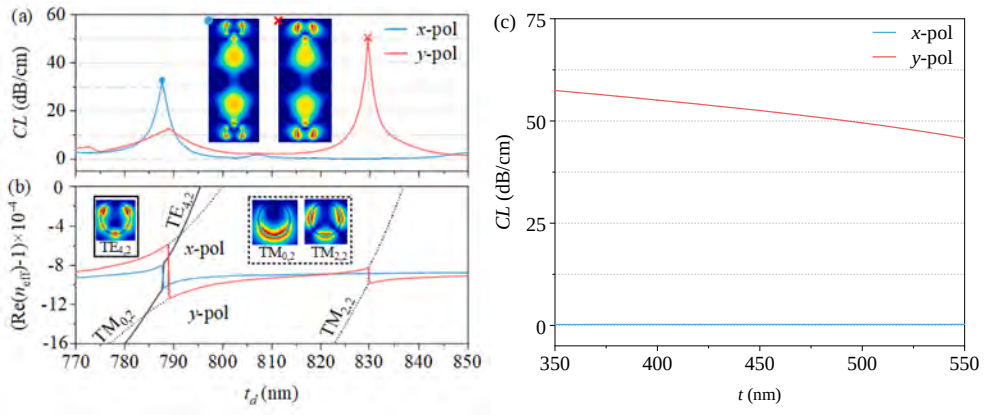

Fig. 2. Variations of CL_x and CL_y with t_d at the wavelength of 1550 nm (a), and Re(n_{eff}) of the *x*-pol mode, *y*-pol mode, and dielectric modes with the modal fields of the dielectric modes shown in the insets (b); variations of CL_x and CL_y with t at the wavelength of 1550 nm (c).

(n_{eff}) curves of the *x*-pol, *y*-pol and dielectric modes ($TE_{4,2}$, $TM_{0,2}$, and $TM_{2,2}$) in Fig. 2(b), the dielectric modes will be excited and coupled with the *x*- or *y*-pol modes by varying t_d. At t_d = 787.6 nm, the *x*-pol mode couples with the $TE_{4,2}$ mode to produce a high CL_x of 32.76 dB/cm. Additionally, even if the $TM_{0,2}$ mode couples with the *y*-pol mode, the resulting CL_y of 12.54 dB/cm at t_d = 789.2 nm is still lower than CL_x at t_d = 787.6 nm. At t_d = 830 nm, the mode coupling between *y*-pol and $TM_{2,2}$ modes causes CL_y to increase to 50.44 dB/cm, while the CL_y exceeds CL_x of 0.25 dB/cm. Therefore, by adjusting the cladding wall thickness t_d, the *x*-pol mode can retain the low loss, but the *y*-pol mode can be filtered.

In addition, the effect of the wall thickness t of cladding tubes in the *x*-direction on CL_x and CL_y is analyzed. When the t_d is 830 nm, variations of CL_x and CL_y with the change in t are shown in Fig. 2(c). It can be observed that the CL_y is significantly higher than CL_x in the range of t from 350 nm to 550 nm. With the increase of t, the CL_y decreases from 57.5 dB/cm to 45.8 dB/cm, whereas the CL_x remains almost constant around 0.26 dB/cm. It is evident that the t_d has a much greater impact on the polarization filtering characteristics of the fiber than the t.

3. Numerical analysis

According to the analysis presented above, the wall thickness t_d of the fiber plays an important role in determining the modal characteristics of the DHC-ARF for the SP coupler. In particular, the high *CL* primarily depends on the mode coupling between the core modes and dielectric modes in the fiber. However, the core diameter D and cladding tube diameter d also affect the mode coupling and therefore, the influence of D, d, and t_d on the two polarized modes is analyzed at 1550 nm.

3.1. Impact of D, d, and t_d on the y-pol mode

Because the primary aim of designing the DHC-ARF is to filter the *y*-pol mode, the influence of D, d, and t_d on CL_y is first assessed. Fig. 3 shows that the CL_y varies with d and t_d for D = 20 μm, 25 μm, and 30 μm. The CL_y can be increased for different D by adjusting d and t_d and exhibits a similar trend when d increases from 10 μm to 16 μm and t_d decreases from 0.86 μm to 0.80 μm. In order to analyze the variation of the high CL_y for different D, we mark the high CL_y with the black curves for different D in Fig. 3. The highest CL_y lies in the black curves and is marked by "+". For D = 20 μm, the largest CL_y is 81.82 dB/cm at d = 10.75 μm and t_d = 0.845 μm. For D = 25 μm, the largest CL_y is 50.44 dB/cm at d = 12.5 μm and t_d = 0.830 μm. For D = 30 μm, the largest CL_y is 30.71 dB/cm at d = 14.25 μm and t_d = 0.818 μm. The largest CL_y decreases with the increase of D because the mode coupling between *y*-pol mode and dielectric mode weakens as D increases. To obtain the DHC-ARF with a high CL_y, a smaller core diameter D should be selected.

3.2. Impact of D, d, and t_d on the x-pol mode

As the *x*-pol mode is set as the primary ESOP, the influence of D, d, and t_d on the *x*-pol mode is evaluated. Fig. 4 shows the influence of d and t_d on CL_x for D = 20 μm, 25 μm, and 30 μm. As it is necessary to reduce CL_x under a high CL_y, the variations of CL_x with d and t_d for different D as well as the high CL_y marked by the black curves are given. The white line represents CL_x = 0.5 dB/cm. The region of low CL_x below 0.5 dB/cm expands with increasing D, while the high CL_y curve crosses the region of low CL_x for different D. The highest CL_y marked by "+" is located in the region of low CL_x. The low CL_x corresponding to the highest CL_y is also marked by "+" in Fig. 4. From Fig. 3 and Fig. 4, it can be concluded that the highest CL_y is 81.82 dB/cm and the corresponding CL_x is 0.40 dB/cm for D = 20 μm; the highest CL_y is 50.44 dB/cm and the corresponding CL_x is 0.24 dB/cm for D = 25 μm; the highest CL_y is 30.71 dB/cm and the corresponding CL_x is 0.17 dB/cm for D = 30 μm. Therefore, CL_x decreases with increasing D because a larger D suppresses the leakage of the *x*-pol mode into the cladding tubes leading to the reduced CL_x. The results show that a low CL_x and a high CL_y can be maintained for different D, but to reduce CL_x further, a larger core diameter D should be

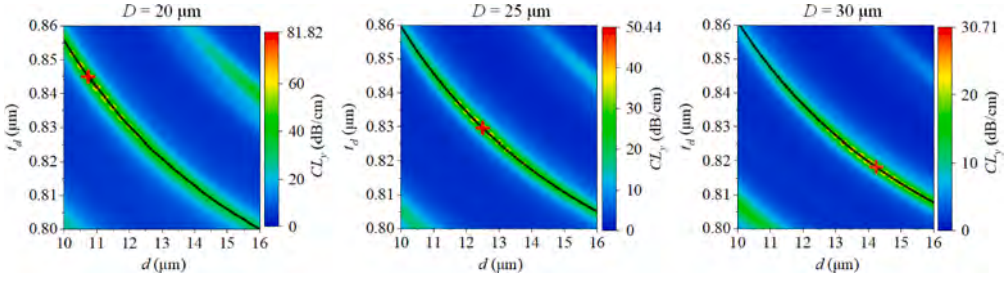

Fig. 3. Variations of CL_y with t_d and d for D = 20 μm, 25 μm, and 30 μm.

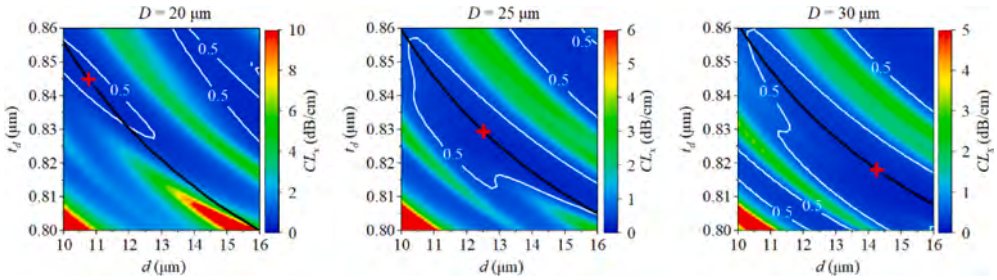

Fig. 4. Variations of CL_x with t_d and d for D = 20 μm, 25 μm, and 30 μm.

selected.

The component length of the coupler based on the dual-core fiber is usually proportional to the L_c of a fiber and affects the characteristics of the coupler such as loss and CR. Therefore, the influence of D, d, and t_d on L_c^x is analyzed. Fig. 5 shows the variation of L_c^x with D, d, and t_d. The high CL_y curve and the highest CL_y marked by "+" are also shown in Fig. 5, in which the white line indicates L_c^x = 5 cm. The highest CL_y marked by "+" lies in the area where L_c^x is less than 5 cm, indicating that the coupler with a short component length can be developed. At the highest CL_y, the corresponding L_c^x is 2.29 cm for D = 20 μm, the corresponding L_c^x is 3.05 cm for D = 25 μm, and the corresponding L_c^x is 3.92 cm for D = 30 μm. The L_c^x at the highest CL_y increases with the increment of D mainly because a larger D increases the distance between the two cores. To reduce the component length, a smaller core diameter D is preferred.

4. DHC-ARF-based SP coupler

According to the above analysis, t_d, t, d, D, and d_s are set to be 0.83 μm, 0.5 μm, 12.5 μm, 25 μm, and 6.8 μm, respectively. To obtain an SP coupler with a CR of 3 dB, the PER of the coupler is supposed to be less than −20 dB to ensure the SP operation, while the CR of a coupler is expected to be limited in the range from 48 % to 52 %. The PER denotes the suppression of the secondary ESOP at the output end of the SP coupler, and the CR is the power ratio of the primary ESOP at the output end of the SP coupler. Because the x-pol mode and y-pol mode are set to be the primary ESOP and secondary ESOP, the PER and CR are expressed as shown in the following:

$$\mathrm{PER} = 10\lg\left(P_B^y/P_B^x\right) \tag{3}$$

$$\mathrm{CR_A{:}CR_B} = \frac{P_\mathrm{A}^x}{P_\mathrm{A}^x + P_\mathrm{B}^x} \times 100\% : \frac{P_\mathrm{B}^x}{P_\mathrm{A}^x + P_\mathrm{B}^x} \times 100\% \tag{4}$$

where $P_\mathrm{A}^{x(y)}$ is the output power of the $x(y)$-pol mode in the incident core A, $P_\mathrm{B}^{x(y)}$ is the output power of the $x(y)$-pol mode in the coupled core B, $\mathrm{CR_A}$ is the CR of the x-pol mode of core A, and $\mathrm{CR_B}$ is the CR of the x-pol mode of core B. $P_\mathrm{A}^{x(y)}$ and $P_\mathrm{B}^{x(y)}$ can be calculated by [32]:

$$P_A^{x(y)} = P_0^{x(y)}\left[\cos\left(\pi L/2L_c^{x(y)}\right)e^{-\alpha_{x(y)}L}\right]^2 \tag{5}$$

$$P_B^{x(y)} = P_0^{x(y)}\left[\sin\left(\pi L/2L_c^{x(y)}\right)e^{-\alpha_{x(y)}L}\right]^2 \tag{6}$$

where $P_0^{x(y)}$ is the input normalized power of the $x(y)$-pol mode and L is the propagation length.

The variations of CL_x and CL_y with wavelength are displayed in Fig. 6 (a). CL_y exceeds 20 dB/cm in the wavelength range between 1547 nm and 1553 nm with a peak value of 50.44 dB/cm at 1550 nm. In contrast, CL_x is lower than 0.27 dB/cm between 1547 nm and 1553 nm. Fig. 6(b) shows the change of L_c of x-pol mode of the fiber with wavelengths. Because the x-pol mode is the primary ESOP, only the L_c^x is given. The L_c^x decreases from 3.15 cm to 2.95 cm in the wavelength region between 1530 nm and 1570 nm and hence, L_c^x exhibits a weak dependence on wavelengths. Owing to the high CL_y, low CL_x, as well as weak wavelength dependence of L_c^x in the wavelength range between 1547 nm and 1553 nm, the DHC-ARF is promising for the SP coupler.

To illustrate the operation of an SP coupler composed of the DHC-ARF, the properties of the DHC-ARF at 1550 nm are determined as

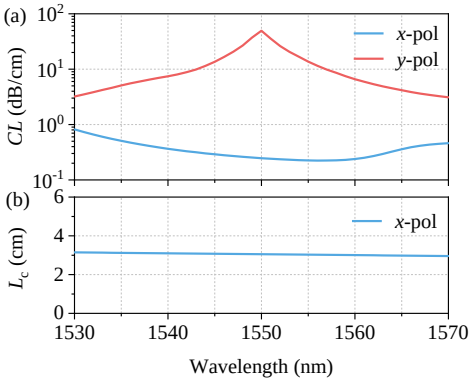

Fig. 6. Variations of CL_x and CL_y (a) and L_c^x (b) with wavelength.

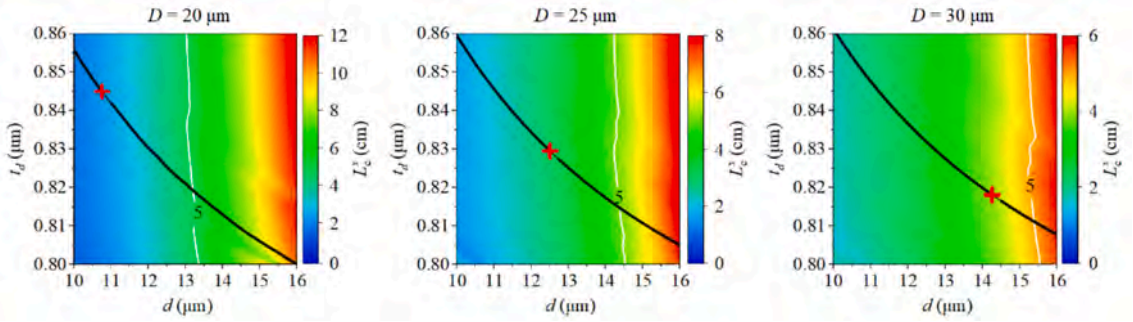

Fig. 5. Variations of L_c^x with t_d and d for D = 20 μm, 25 μm and 30 μm.

shown in Fig. 7. When light is coupled into core A, Fig. 7(a) shows the normalized propagation power of the *x*- and *y*-pol modes in incident core A and coupled core B for a propagation length of 6 cm. The normalized power is calculated by Eqs. (5) and (6). It is evident that both the *x*- and *y*-pol modes can be coupled between the two cores, but the power of the *y*-pol mode decays rapidly with increasing propagation length. To analyze the filtering effect on *y*-pol mode during transmission, the variation of PER with propagation length *L* is shown in Fig. 7(b). PER declines with the increment of *L* and when the *L* is bigger than 0.05 cm, PER is less than −20 dB. Consequently, the fiber can effectively filter the *y*-pol mode when the fiber length is over 0.05 cm. Fig. 7(c) shows the variations of CR_A and CR_B with the propagation length *L* and the grey solid line indicates that CR is 50 %. When the *L* is 1.52 cm or 4.58 cm, $CR_A = CR_B = 50$ % can be obtained at 1550 nm. Therefore, by using the DHC-ARF with a length of 1.52 cm or 4.58 cm, an SP coupler with a CR of 50 % can be obtained at 1550 nm. To reduce the component length, the fiber length is selected to be 1.52 cm.

The characteristics of the SP coupler comprising the 1.52 cm long DHC-ARF are determined for different wavelengths together with PER, CR and loss. Fig. 8(a-1) shows the variations of PER with the propagation length *L* between 1530 nm and 1570 nm. PER decreases with increasing *L* and the lowest PER is observed at 1550 nm for different *L*. The dashed line denotes a coupler length of 1.52 cm. The change of PER with wavelength of the 1.52 cm long coupler is shown in Fig. 8(a-2). In the wavelength range from 1545 nm to 1556 nm, PER is less than −20 dB and the lowest PER of −91.7 dB is obtained at 1550 nm. The change of CR with the propagation length *L* and wavelength is presented in Fig. 8(b-1). CR_B is taken as an example to analyze the CR of an SP coupler. The two white solid lines indicate the CR of 48 % and 52 %, respectively, and the dashed line represents a coupler length of 1.52 cm. In the *L* between 1.2 cm and 1.8 cm, CR increases monotonically with increasing *L* in the wavelength range from 1530 nm to 1570 nm. The changes of CR_A and CR_B with wavelengths of the 1.52 cm long coupler are shown in Fig. 8(b-2). In the wavelength range between 1545 nm and 1556 nm, CR_A decreases from 50.5 % to 49.4 %, and CR_B increases from 49.5 % to 50.6 %. At the wavelength of 1550 nm, CR_A and CR_B are 50 %. The loss of the coupler is also shown in Fig. 8(b-2). Since the *x*-pol mode is the primary ESOP, the loss of the coupler is mainly determined by the CL_x. In the wavelength range between 1545 nm and 1556 nm, the loss of the coupler decreases from 0.44 dB to 0.34 dB. Consequently, when the 1.52 cm long fiber is used as the SP coupler, the operational bandwidth is 11 nm between 1545 nm and 1556 nm, where PER is less than −20 dB, the loss is lower than 0.44 dB, and CR stabilizes to 50 ± 0.6 %. The smallest PER of −91.7 dB is observed at 1550 nm, in which shows a CR of 50 % and loss of 0.37 dB.

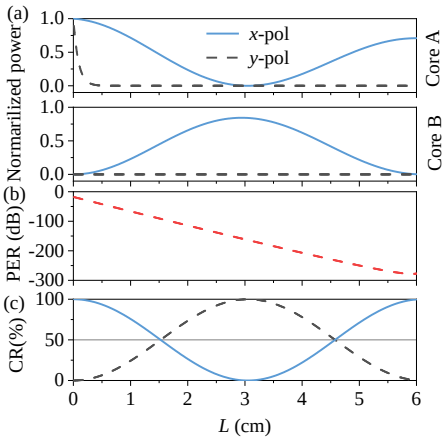

Fig. 7. Variations of the normalized power of the *x*(*y*)-pol mode in cores A and B (a), PER (b) and CR (c) with a propagation length *L* at 1550 nm.

5. Empirical formula

The development of a high-performances SP coupler hinges on the high CL_y and low CL_x of the DHC-ARF and the structural parameters are optimized for the wavelength of 1550 nm. High CL_y originates from the mode coupling between *y*-pol mode and dielectric mode. The dielectric mode is closely related to the wall thickness t_d and the diameter *d* of cladding tubes located in the *y*-direction, and is slightly affected by the core diameter *D*. Therefore, we focus on investigating the impact of the t_d and *d* on the *CL* of the fiber for different wavelengths and derive the empirical formulas to predict the structural parameters of the DHC-ARF for the SP coupler.

5.1. Empirical formula for λ

Since t_d is important to *CL* at the expected wavelength, we first analyze the impact of t_d on *CL* at different wavelengths for $D = 25$ μm and $d = 12.5$ μm. According to the analysis in subsection 3.2, CL_x is lower than CL_y in the high-loss region of CL_y and therefore, we analyze the effect of t_d on *CL* through the difference between CL_y and CL_x (CL_y - CL_x). When the wavelength λ changes from 1.05 μm to 2.0 μm with a step of 0.05 μm, the variation of CL_y - CL_x with t_d is shown in Fig. 9(a). Because the high PER of an SP coupler mainly benefits from the high CL_y, only the curves of CL_y - CL_x over 0 dB/cm are shown in Fig. 9(a). A high CL_y - CL_x can be obtained at different wavelengths by tuning t_d. For example, to obtain the highest CL_y - CL_x at 1.4 μm or 1.9 μm, t_d for the DHC-ARF with $D = 25$ μm and $d = 12.5$ μm should be 0.7388 μm or 1.0518 μm, respectively.

Next, we study the relationship between t_d at the highest CL_y - CL_x and wavelength. The simulation results of t_d at the highest CL_y - CL_x for different wavelengths are denoted by the discrete points as shown in Fig. 9(b). It can be seen that t_d increases approximately linearly with wavelength except in the resonant region. By fitting the discrete points, the empirical formula $t_d = 0.617\lambda - 0.126$ is derived in order that t_d can be predicted at the highest CL_y - CL_x for different wavelengths. At the wavelength of 1.4 μm, the predicted t_d is 0.7378 μm and the simulated t_d is 0.7388 μm. At the wavelength of 1.9 μm, the predicted t_d is 1.0463 μm and the simulated t_d is 1.0518 μm. Hence, the predicted t_d is very close to the simulated t_d and t_d at high CL_y - CL_x at different wavelengths can be predicted by this empirical relationship.

We then evaluate the performance of two kinds of SP couplers, one of which is based on the DHC-ARF with t_d obtained from the empirical formula $t_d = 0.617\lambda - 0.126$ and the other based on the DHC-ARF with simulated t_d. At 1.4 μm, the predicted and simulated t_d values are 0.7378 μm and 0.7388 μm, respectively. By using the 1.53 cm long DHC-ARF with $t_d = 0.7378$ and a 1.53 cm long DHC-ARF with $t_d = 0.7388$ μm, the two couplers are analyzed as shown in Fig. 10(a-c). For the predicted $t_d = 0.7378$ μm, the PER, CR_A, CR_B, and loss are −27.85 dB, 49.71 %, 50.29 %, and 0.31 dB at 1.4 μm, respectively, while for the simulated $t_d = 0.7388$ μm, the PER, CR_A, CR_B, and loss are −67.44 dB, 50 %, 50 %, and 0.33 dB at the same wavelength, respectively. By comparing the characteristics of the SP coupler with the predicted $t_d = 0.7378$ μm with those of that one with the simulated $t_d = 0.7388$ μm, the properties of the former degrade, but PER is still lower than −20 dB and the SP characteristics can be maintained at 1.4 μm. We then evaluate the performance of the SP couplers for the predicted $t_d = 1.0463$ μm and simulated $t_d = 1.0518$ μm at the wavelength of 1.9 μm as shown in Fig. 10(d–f). For the predicted $t_d = 1.0463$ μm, the PER, CR_A, CR_B, and loss of the 1.41 cm long DHC-ARF-based coupler are –23.18 dB, 50.58 %, 49.42 %, and 0.48 dB at 1.9 μm, while for the simulated $t_d = 1.0518$ μm, the PER, CR_A, CR_B, and loss of the 1.41 cm long DHC-ARF-based coupler are −63.36 dB, 50 %, 50 %, and 0.49 dB at the same wavelength, respectively. Therefore, the SP coupler can be analyzed by the same empirical formula at 1.9 μm. For $D = 25$ μm and $d = 12.5$ μm, t_d of the DHC-ARF at the expected wavelength can be derived.

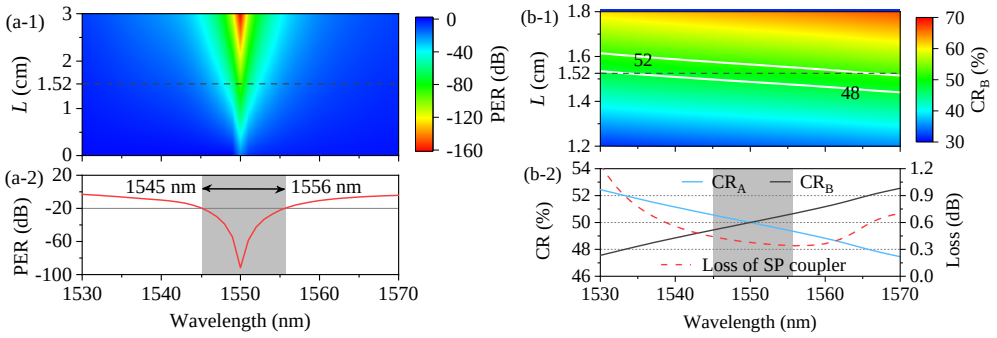

Fig. 8. Variations of PER (a-1), and CR (b-1) with L and wavelength; variations of PER (a-2), and CR_A, CR_B, and loss (b-2) with wavelength for the 1.52 cm long-DHC-ARF-based SP coupler.

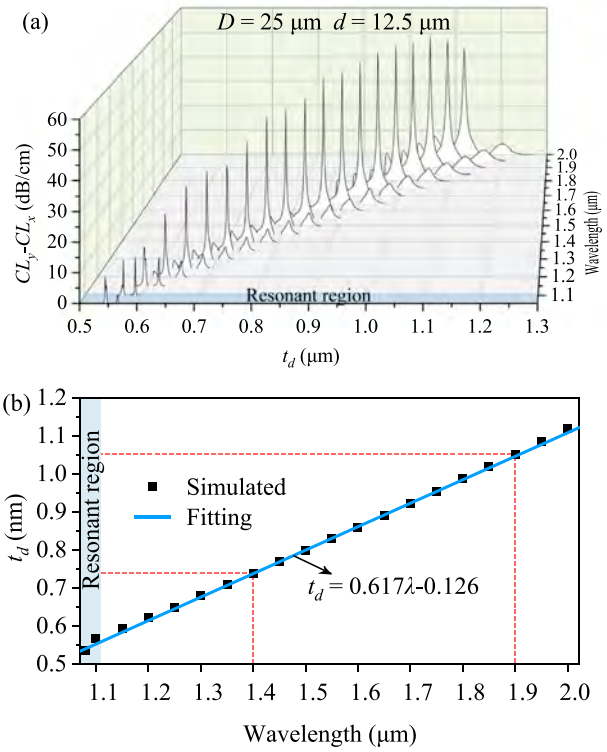

Fig. 9. Variations of CL_y - CL_x with t_d for different wavelengths (a), and t_d at the highest CL_y - CL_x (discrete points) for different wavelengths with the fitted curve (b).

5.2. Empirical formula for λ and d

According to Section 3, it is evident that CL_y and CL_x not only depend on t_d, but are also influenced by the diameter of the cladding tubes d and we further analyze the impact of t_d, d, and wavelength λ on CL_y - CL_x for $D = 25$ μm. When the wavelength changes from 1.25 μm to 2.0 μm with a step of 0.15 μm and d varies from 11 μm to 17 μm with a step of 1 μm, the variations of t_d at the highest CL_y - CL_x with λ and d are derived and presented in Fig. 11, in which t_d at the highest CL_y - CL_x is denoted by discrete points. By fitting the discrete points, the empirical formula of $t_d = 0.728d / (d\text{-}1.53) + 0.617\lambda - 0.956$ can be derived. Hence, t_d at the highest CL_y - CL_x can be predicted for different λ and d. For example, for $\lambda = 1.25$ μm and $d = 11$ μm, $\lambda = 1.55$ μm and $d = 14$ μm, $\lambda = 1.70$ μm and $d = 14$ μm, $\lambda = 2.0$ μm and $d = 17$ μm, $\lambda = 2.0$ μm and $d = 11$ μm, as well as $\lambda = 1.25$ μm and $d = 17$ μm, the six predicted t_d are 0.6609 μm, 0.8177 μm, 0.9102 μm, 1.0780 μm, 1.1236 μm, and 0.6152 μm, which are labeled with red "×" in Fig. 11. The six simulated t_d values are 0.6605 μm, 0.8170 μm, 0.9080 μm, 1.0644 μm, 1.1490 μm, and 0.6326 μm. It can be seen that the six predicted t_d obtained by the empirical formula are very close to the six simulated t_d.

Next, we compare the properties of the two SP couplers, one of which is based on the DHC-ARF with predicted t_d and the other based on the DHC-ARF with simulated t_d. The characteristics of the two SP couplers based on the predicted fiber and simulated fiber are given in Table 1 for $\lambda = 1.25$ μm and $d = 11$ μm, $\lambda = 1.55$ μm and $d = 14$ μm, $\lambda = 1.70$ μm and $d = 14$ μm, $\lambda = 2.0$ μm and $d = 17$ μm, $\lambda = 2.0$ μm and $d = 11$ μm, as well as $\lambda = 1.25$ μm and $d = 17$ μm. The corresponding component lengths derived by simulation are 1.06 cm, 2.25 cm, 2.21 cm, 4.69 cm, 0.96 cm, and 4.07 cm, respectively. For the first four sets of λ and d ($\lambda = 1.25$ μm and $d = 11$ μm, $\lambda = 1.55$ μm and $d = 14$ μm, $\lambda = 1.70$ μm and $d = 14$ μm, and $\lambda = 2.0$ μm and $d = 17$ μm), the SP coupler with PER below −20 dB and CR stabilizing around 50 % can be developed by using the formula at the expected wavelength, even if the SP characteristics degrade compared to the SP coupler based on the simulated fiber. However, for the last two sets of λ and d ($\lambda = 2.0$ μm and $d = 11$ μm, and $\lambda = 1.25$ μm and $d = 17$ μm), the SP coupler based on the predicted fiber shows a PER over −20 dB and a CR deviating from 50 %, indicating that the properties of the SP coupler based on predicted fiber degrade when d decreases and λ increases, or when d increases and λ decreases. To obtain the SP coupler at the expected wavelength using the empirical formula, a smaller d should be selected at short wavelengths and a larger d should be selected at long wavelengths. By using the empirical formula, t_d of the DHC-ARF for different d and λ can be predicted to aid the development of the DHC-ARF-based SP coupler.

6. Fabrication tolerance

The fabrication tolerance of structural parameters can characterize the impact of small changes of the structure during manufactured process on the performance of an SP coupler. The thickness t and diameter d of the cladding tube have significant deviations during the manufacturing process, so the performance of an SP coupler is analyzed within the ± 1 % fabrication tolerance of t and d (Δt and Δd). The cladding tube in the y-direction has a relative thick wall thickness t_d, which undergoes a relative small deformation during the manufactured process. Therefore, the impact of fabrication tolerances of t and d on the performance of the SP coupler is summarized in Table 2. The results show that the bandwidth, the lowest PER, and CR are all within acceptable ranges at the t and d with ± 1 % change, which indicates that the SP coupler exhibits high-performance in stability.

7. Conclusion

An SP coupler based on a DHC-ARF is designed and analyzed. By using cladding tubes with two different wall thicknesses along the two orthogonal directions, one polarized mode can be filtered out due to its

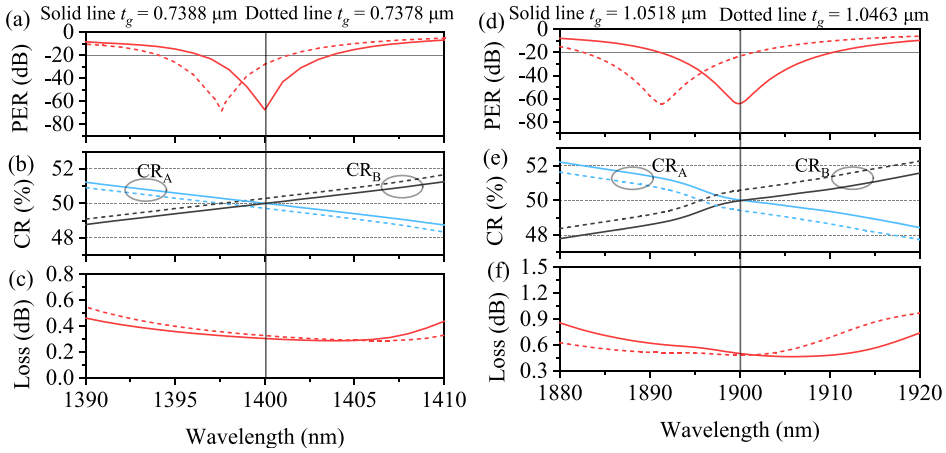

Fig. 10. For D = 25 μm, d = 12.5 μm and, t_g = 0.7388 μm and 0.7378 μm, variations of PER (a), CR (b) and loss (c) with wavelengths; for D = 25 μm, d = 12.5 μm, and t_g = 1.0518 μm and 1.0463 μm, variations of PER (d), CR (e) and loss (f) with wavelengths.

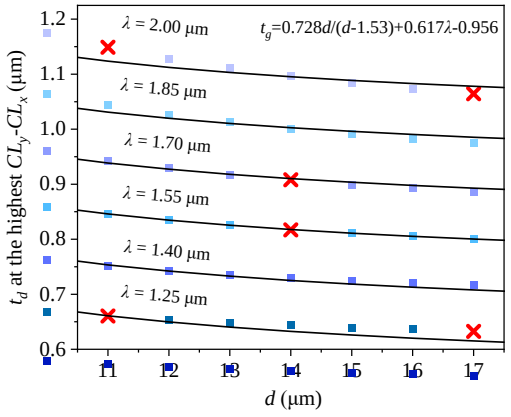

Fig. 11. t_d at the highest CL_y - CL_x (discrete points) and fitted curves for different wavelengths.

high CL caused by the mode coupling with the dielectric modes in the cladding wall, while another polarized mode with a low CL is maintained. Numerical results shows that the CL of the high-loss polarized mode is 50.44 dB/cm, but that of the low-loss polarized mode is only 0.24 dB/cm at 1550 nm through optimizing the structural parameters. By using a 1.52 cm long DHC-ARF, the SP coupler shows an operational bandwidth of 11 nm thus covering the wavelength range between 1545 nm and 1556 nm. The PER is less than −20 dB, the CR is stable at 50 ± 0.6 %, and the loss is less than 0.44 dB. At the wavelength of 1550 nm, the lowest PER of the coupler is −91.7 dB, while the CR and loss are 50 % and 0.44 dB, respectively. By analyzing the structural parameters of the fiber, empirical formulas are derived for the structure and wavelength, and based on the empirical formulas, the SP coupler composed of the DHC-ARF can be predicted at the expected wavelengths. At the t and d with ± 1 % change, the SP coupler exhibits high-performance in stability.

Funding

This work was supported by Beijing Municipal Natural Science Foundation (1232028); National Natural Science Foundation of China (NSFC) (12174022).

CRediT authorship contribution statement

Donglian Hou: Data curation, Investigation, Validation, Visualization, Writing – original draft. **Haoqiang Jia:** Conceptualization, Data curation, Investigation, Methodology, Software, Validation, Visualization, Writing – original draft. **Xing Wang:** Writing – review & editing, Supervision. **Xinzhi Sheng:** Writing – review & editing, Supervision. **Lu Xue:** Writing – review & editing, Supervision. **Paul K. Chu:** Writing – review & editing, Supervision. **Shuqin Lou:** Writing – review & editing.

Table 2
Performance of the SP coupler at different fabrication tolerance.

Parameter	Tolerance	Operating wavelengths	Bandwidth	Lowest PER	CR
Δt	−1%	1545–1555 nm	10 nm	81.7 dB	50 ± 0.7 %
	+1%	1545–1555 nm	10 nm	81.0 dB	50 ± 0.7 %
Δd	−1%	1544–1553 nm	9 nm	77.9 dB	50 ± 0.6 %
	+1%	1547–1556 nm	9 nm	72.5 dB	50 ± 0.6 %

Table 1
Characteristics of the SP couplers based on the six DHC-ARFs with predicted t_d and simulated t_d.

d and λ (μm)	Couplers based on predicted fibers				Couplers based on simulated fibers			
	t_d (μm)	PER (dB)	CR_A (%)	Loss (dB)	t_d (μm)	PER (dB)	CR_A (%)	Loss (dB)
λ = 1.25 and d = 11	0.6609	−23.95	50.11	0.32	0.6605	−51.86	50	0.32
λ = 1.55 and d = 14	0.8177	−73.82	50.16	0.46	0.8170	−78.14	50	0.48
λ = 1.70 and d = 14	0.9102	−45.16	50.398	0.61	0.9080	−101.06	50	0.58
λ = 2.00 and d = 17	1.0780	−28.63	53.130	3.08	1.0644	−196.00	50	8.14
λ = 2.00 and d = 11	1.1236	−2.76	60.086	0.54	1.1490	−21.31	50	0.59
λ = 1.25 and d = 17	0.6152	1.87	38.06	20.61	0.6326	−56.55	50	1.39

Declaration of competing interest

The authors declare that they have no known competing financial interests or personal relationships that could have appeared to influence the work reported in this paper.

Data availability

Data will be made available on request.

References

[1] G.A. Sanders, A.A. Taranta, C. Narayanan, et al., Hollow-core resonator fiber optic gyroscope using nodeless anti-resonant fiber, Opt. Lett. 46 (1) (2021) 46–49.
[2] R. Carroll, C. Coccoli, D. Cardarelli, et al., The Passive resonator fiber optic gyro and comparison to the interferometer fiber gyro, in Fiber Optic Gyros: 10th Anniversary Conference, SPIE, 1987.
[3] Y. Zhang, Z. Wang, G. Wang, et al., Polarization stability of spun fiber resonator for resonant fiber optic gyro, IEEE Sens. J. 23 (14) (2023) 15644–15651.
[4] W. Fan, X. She, H. Shen, et al., Ring resonator of hollow-core photonic crystal fiber based on spatial coupling scheme, J. Lightwave Technol. 41 (16) (2023) 5468–5474.
[5] L. Feng, X. Ren, X. Deng, et al., Analysis of a hollow core photonic bandgap fiber ring resonator based on micro-optical structure, Opt. Express 20 (16) (2012) 18202–18208.
[6] K. Iwatsuki, M. Higashiguchi, Effect of Rayleigh backscattering in an optical passive ring-resonator gyro, Appl. Opt. 23 (21) (1984) 3916–3924.
[7] K. Iwatsuki, M. Higashiguchi, Eigenstate of polarization in a fiber ring resonator and its effect in an optical passive ring-resonator gyro, Appl. Opt. 25 (15) (1986) 2606–2612.
[8] K. Iwatsuki, M. Higashiguchi, Kerr effect in an optical passive ring-resonator gyro, J. Lightwave Technol. 4 (6) (1986) 645–651.
[9] X. Suo, H. Yu, J. Li, et al., Transmissive resonant fiber-optic gyroscope employing kagome hollow-core photonic crystal fiber resonator, Opt. Lett. 45 (8) (2020) 2227–2230.
[10] H. Jiao, L. Feng, N. Liu, et al., Improvement of long-term stability of hollow-core photonic-crystal fiber optic gyro based on single-polarization resonator, Opt. Express 26 (7) (2018) 8645–8655.
[11] R.E. Meyer, S. Ezekiel, D.W. Stowe, et al., Passive fiber-optic ring resonator for rotation sensing, Opt. Lett. 8 (12) (1983) 644–646.
[12] A.M. Smith, Birefringence induced by bends and twists in single-mode optical fiber, Appl. Opt. 19 (15) (1980) 2606–2611.
[13] K. Takiguchi, K. Hotate, Reduction of a polarization-fluctuation-induced error in an optical passive ring-resonator gyro by using a single-polarization optical fiber, J. Lightwave Technol. 11 (10) (1993) 1687–1693.
[14] X. Wang, Z. He, K. Hotate, Reduction of polarization-fluctuation induced drift in resonator fiber optic gyro by a resonator with twin 90° polarization-axis rotated splices, Opt. Express 18 (2) (2010) 1677–1683.
[15] H. Cai, F. Yu, M. Liao, et al., Thin-diameter polarization maintaining hollow-core photonic bandgap fiber for fiber optic gyroscope, Opt. Fiber Technol. 55 (2020) 102141.
[16] H. Ma, Z. Chen, Z. Jin, Single-polarization coupler based on air-core photonic bandgap fibers and implications for resonant fiber optic gyro, J. Lightwave Technol. 32 (1) (2014) 46–54.
[17] R. Dyott, V. Handerek, J. Bello, Polarization holding directional couplers using D fiber, in 1984 Technical Symposium East, SPIE, 1984.
[18] Z. Xu, X. Li, C. Zhang, et al., Design of single-polarization coupler based on dual-core photonic band-gap fiber implied in resonant fiber optic gyro, Opt. Commun. 380 (2016) 302–309.
[19] J. Lou, T. Cheng, S. Li, Ultra-short polarization beam splitter with square lattice and gold film based on dual-core photonic crystal fiber, Optik 179 (2019) 128–134.
[20] S. Lou, Z. Tang, L. Wang, Design and optimization of broadband and polarization-insensitive dual-core photonic crystal fiber coupler, Appl. Opt. 50 (14) (2011) 2016–2023.
[21] H. Jia, X. Wang, T.M. Benson, et al., Ultrawide bandwidth dual sakura hollow-core antiresonant fiber polarization beam splitter, J. Opt. Soc. Am. B 38 (11) (2021) 3395–3402.
[22] K.S.R. Shaha, A. Khaleque, M.T. Rahman, et al., Broadband and short-length polarization splitter on dual hollow-core antiresonant fiber, IEEE Photonics Tech. l. 34 (5) (2022) 259–262.
[23] S. Lou, H. Jia, D. Hou, et al., Ultra-broadband 3-dB coupler based on dual-hollow-core polymer fiber covering E + S + C + L + U band, Opt. Express 31 (18) (2023) 29877–29886.
[24] H. Jia, X. Wang, S. Gu, et al., Decoupling of dual-hollow-core anti-resonant fiber, Optik 273 (2023) 170495.
[25] H. Jia, X. Wang, B. Huang, et al., Compact single-polarization coupler based on a dual-hollow-core anti-resonant fiber, Opt. Express 31 (8) (2023) 12410–12422.
[26] Z. Wang, G. Kai, Y. Liu, et al., Coupling and decoupling of dual-core photonic bandgap fibers, Opt. Lett. 30 (19) (2005) 2542–2544.
[27] V. Serrão, M. Franco, Single-polarization single-mode hollow core photonic bandgap fiber for gyroscope applications, in International Conference on Optical Fibre Sensors, SPIE, 2015.
[28] C. Wei, C.R. Menyuk, J. Hu, Polarization-filtering and polarization-maintaining low-loss negative curvature fibers, Opt. Express 26 (8) (2018).
[29] S. Yan, S. Lou, W. Zhang, et al., Single-polarization single-mode double-ring hollow-core anti-resonant fiber, Opt. Express 26 (24) (2018) 9528–9540.
[30] M.A. Mollah, S. Rana, H. Subbaraman, Polarization filter realization using low-loss hollow-core anti-resonant fiber in THz regime, Results Phys. 17 (2020) 103092.
[31] J. Zang, C. Goel, M.R.A. Hassan, et al., Antiresonant hollow-core inline fiber polarizer, J. Lightwave Technol. 40 (16) (2022) 5689–5697.
[32] P. Li, J. Zhao, Polarization-dependent coupling in gold-filled dual-core photonic crystal fibers, Opt. Express 21 (5) (2013) 5232–5238.